# Coordinated Reconfigurable Intelligent Surface for Cellular-Connected UAV

Wee Kiat New[†], Chee Yen Leow[‡], Chuan Heng Foh[*], Kai-Kit Wong[†], Hao Xu[†], Farshad Rostami Ghadi[†]

[†]Department of Electronic and Electrical Engineering, University College London, London, WC1E 7JE, United Kingdom.

[‡]Wireless Communication Centre, Faculty of Electrical Engineering, Universiti Teknologi Malaysia, 81310 Skudai, Johor, Malaysia.

[*]5GIC and 6GIC Institute for Communication Systems (ICS), University of Surrey, Guildford, GU2 7XH, United Kingdom.

Email: {a.new, kai-kit.wong, hao.xu, f.rostamighadi}@ucl.ac.uk; bruceleow@utm.my; c.foh@surrey.ac.uk.

***Abstract*—Inter-cell interference (ICI) and limited sky coverage are major challenges to the development of cellular-connected unmanned aerial vehicle (UAV). To address these challenges, we consider the applications of reconfigurable intelligent surface (RIS). RIS is a promising solution capable of reconfiguring the phase of a reflected radio signal so as to enhance the desired signal strength or mitigate the ICI. In this paper, we propose a coordinated RIS-aided cellular-connected UAV scheme to provide ubiquitous coverage in the sky and mitigate the ICI of aerial users (AUs) while improving the performance of existing terrestrial users (TUs). We further develop an optimization algorithm to obtain the optimal coordinated beamforming and phase shift that maximize the weighted sum-rate (WSR) of the TUs subject to the AUs' rate requirement. Our simulation results show that the proposed coordinated RIS-aided cellular-connected UAV scheme is a promising solution where the WSR of the TUs increases with respect to the number of reflecting elements while satisfying the AUs' rate requirement. Compared to the baseline scheme without RIS, the proposed scheme also provides a WSR gain up to 48%.**

***Index Terms*—Cellular-Connected UAV, Reconfigurable Intelligent Surface, Inter-cell Interference, Weighted Sum-Rate.**

## I. Introduction

Cellular-connected unmanned aerial vehicle (UAV) has garnered significant interest in fifth-generation (5G) and beyond networks [1]. Companies such as Qualcomm, Huawei, Vodafone, and Ericsson have conducted trials to support UAVs as aerial users (AUs) via cellular networks. These connections enable AUs to operate beyond visual line-of-sight (LOS), potentially unlocking a wide range of new UAV applications in agriculture, delivery, construction, sports, entertainment, and industrial services, thereby creating new revenue streams for telecommunications companies.

Nevertheless, serving AUs via cellular networks is a very challenging task. One of the main challenges is limited coverage in the sky [2]. Since the antennas of the BSs are typically downtilted, AUs are served through the sidelobes of the BSs. In some cases, the AUs may even be positioned in the null direction, which can lead to network outages. Another key challenge is strong inter-cell interference (ICI) [3]. In particular, AUs that are hovering at a high altitude experience a higher probability of LOS to the base stations (BSs) [4]. Consequently, AUs suffer strong ICI from neighboring BSs. Thus, researchers are attempting to mitigate the ICI of AUs without significantly affecting the performance of existing terrestrial users (TUs).

To this end, an interference-aware scheme [5], an efficient coordinated multi-point transmission and adaptive receiving scheme [6], and a cooperative beamforming and interference cancellation scheme [7] have been proposed. These schemes are efficient but they require additional specifications or some conditions at the user side. For instance, [5], [6] require specific types of antenna at the AUs, and [7] requires a low user density. A less demanding solution at the user side is clearly desired.

Reconfigurable Intelligent Surface (RIS) has recently emerged as a promising solution for future cellular networks [8]. RIS is a low cost meta-surface consisting of a large number of reflecting elements [9]. The reflecting elements can be active, passive, or hybrid [10]. However, in this paper, we mainly focus on passive reflecting elements. Each of the passive reflecting elements is capable of inducing a certain phase shift to the radio signals [11]. By adjusting the phase shift of these elements, the reflected radio signals can be added constructively or destructively. This enhances the received signal strength and/or suppresses the interference at the intended users.

Several efforts have been made to analyze the performance gains of RIS across various applications and setups. To name a few, [12] considered a single-cell network with a RIS and multiple users, [13] explored multi-cell networks with multiple users and a RIS positioned at the cell boundary, [14] investigated the use of a RIS in an aerial relay setup, and [15] examined the integration of RIS with fluid antennas. Many existing works consider a RIS which is placed near to the users and/or the path loss of the direct links (i.e., BS-to-user link) are more severe than that of the reflected links (i.e., BS-RIS-user links). In some cases, the direct communication links are entirely blocked.

Nevertheless, in cellular-connected UAV, it is difficult to place the RIS near to AUs. Due to high probability of LOS, the direct links might also be stronger than the reflected links. Therefore, it remains uncertain how RIS can be effectively utilized in conjunction with the co-existence of AUs and TUs, particularly in addressing the challenges of limited sky coverage and severe ICI for new AUs without negatively

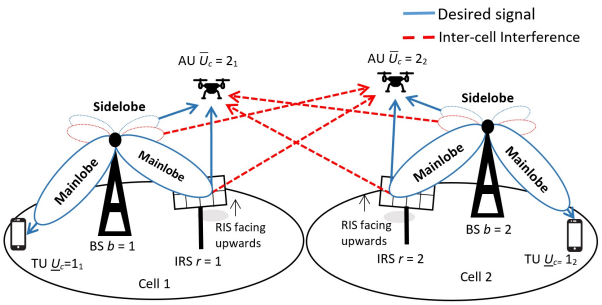


Figure 1. A schematic of the RIS-aided cellular-connected UAV.

impacting the TUs. Furthermore, there may be more than one RIS in the cellular networks. Optimizing the performance for a specific AU could potentially impact the performance of other users. Given these characteristics, the performance gain of coordinated RIS for cellular-connected UAV remains unclear especially for multi-antenna system. Motivated by these factors, we investigate the performance gain of coordinated RIS for cellular-connected UAV in downlink communication.

Specifically, in this paper, we consider multi-cell networks where each BS is equipped with multiple antennas and serves both AUs and TUs simultaneously. Furthermore, each cell consists of a RIS, where the RIS is deploy to provide ubiquitous coverage in the sky and mitigate the strong ICI without negatively impacting the TUs.

Overall, the main contributions of this paper can be summarized as follows:

- We propose a coordinated RIS-aided cellular-connected UAV scheme to provide ubiquitous coverage in the sky and mitigate the strong ICI of AUs while improving the performance of TUs.
- We develop an optimization algorithm to obtain the optimal coordinated beamforming and phase shift that maximize the weighted sum-rate (WSR) of the TUs subject to AUs' rate requirement, where the AUs' rate requirement is used to ensure the safe operation of the AUs.
- Lastly, we provide quantitative insights into the performance gains of the proposed RIS-aided cellular-connected UAV system and discuss the impact of the AUs' locations.

The rest of the paper is organized as follows: Section II discusses the system model, Section III presents the optimal coordinated beamforming and phase shift, and the results are discussed in Section IV. Finally, the conclusion is provided in Section V.

## II. System Model

As shown in Fig. 1, we consider a downlink wireless communication system with multiple terrestrial BSs. Each terrestrial BS forms a cell and is equipped with $M$ transmit antennas, where $M > 1$. We assume each of the cell consists of a RIS with $N$ reflecting elements, $T_c$ single-antenna terrestrial users (TUs), and $A_c$ single-antenna aerial users (AUs).

For ease of expositions, we use the subscript $b \in \mathcal{B} = \{1, \ldots, B\}$, $r \in \mathcal{I} = \{1, \ldots, B\}$, $\underline{u}_c \in \underline{\mathcal{U}}_c = \{1_c, \ldots, T_c\}$, and $\overline{u}_c \in \overline{\mathcal{U}}_c = \{T_c + 1, \ldots, U_c\}$ to denote the index of the BSs, RISs, TUs, and AUs, respectively. Without loss of generality, we assume RIS $r$, TU $\underline{u}_c$ and AU $\overline{u}_c$ are associated to BS $b$ if and only if $r = c = b$. Furthermore, we use the subscript $u_c \in \mathcal{U}_c = \underline{\mathcal{U}}_c \cup \overline{\mathcal{U}}_c$ to denote any types of users.

Furthermore, we consider the associated RIS $r$ is deployed near to BS $b$, where $r = b$, and it is below the BS and facing upwards so that the incident reflected signals impact the AUs only. The reason for such deployment is to ensure the signal enhancement and ICI cancellation only affect the AUs. Specifically, the proposed RIS is used to address the AUs' ICI issue without negatively affecting the performance of the TUs.[1]

The baseband equivalent channels from BS $b$ to RIS $r$, RIS $r$ to AU $\overline{u}_c$, and BS $b$ to AU $\overline{u}_c$ are denoted by $\boldsymbol{F}_{b,r} \in \mathbb{C}^{N \times M}$, $\boldsymbol{g}_{r,\overline{u}_c}^H \in \mathbb{C}^{1 \times N}$, and $\boldsymbol{h}_{b,\overline{u}_c}^H \in \mathbb{C}^{1 \times M}$, respectively. The phase shift and reflection coefficient matrix of RIS $r$ are denoted by $\boldsymbol{\theta}_r = [\theta_{r,1}, \ldots, \theta_{r,N}]$ and $\boldsymbol{\Theta}_r = \text{diag}\left(e^{j\theta_{r,1}}, \ldots, e^{j\theta_{r,N}}\right)$, respectively. The baseband equivalent channel from BS $b$ to TU $\underline{u}_c$ is denoted by $\boldsymbol{h}_{b,\underline{u}_c}^H \in \mathbb{C}^{1 \times M}$. The antennas of the BSs are typically downtilted. Consequently, AUs at high altitudes are served through the sidelobe of the BSs, while RIS and TUs are served through the mainlobe of the BSs [16].

### A. Space Division Multiple Access (SDMA)

We assume the BSs perform linear transmit precoding and each of their associated users is assigned with a beamforming vector. The complex baseband transmitted signal at BS $b$ is $\boldsymbol{x}_b = \sum_{\forall u_b} \boldsymbol{w}_{b,u_b} s_{b,u_b}$, where $s_{b,u_b}$ is the desired message from BS $b$ to its associated user $u_b$, and $\boldsymbol{w}_{b,u_b}$ is the corresponding beamforming vector for user $u_b$. The received signal at AU $\bar{u}_b$ is

$$y_{\bar{u}_b} = \underbrace{\left(\boldsymbol{g}_{r,\bar{u}_b}^H \boldsymbol{\Theta}_r^H \boldsymbol{F}_{b,r}}_{\text{BS-IRS-AU link}} + \underbrace{\boldsymbol{h}_{b,\bar{u}_b}^H}_{\text{BS-AU link}}\right)_{r=b} \boldsymbol{x}_b + \underbrace{\sum_{c \neq b} \left(\boldsymbol{g}_{r,\bar{u}_c}^H \boldsymbol{\Theta}_r^H \boldsymbol{F}_{c,r} + \boldsymbol{h}_{c,\bar{u}_c}^H\right)_{r=c} \boldsymbol{x}_c}_{\text{inter-cell interference}} + n_{\bar{u}_b}, \quad (1)$$

where the first term is the overall channel from BS $b$ and RIS $r = b$, the second term is the aggregated ICI from BS $c \neq b$ and RIS $r \neq b$, and $n_{\bar{u}_b} \sim \mathcal{CN}(0, N_0)$ is the additive white Gaussian noise (AWGN) at AU $\bar{u}_b$. In the first term of (1), $\boldsymbol{g}_{r,\bar{u}_b}^H \boldsymbol{\Theta}_r^H \boldsymbol{F}_{b,r}$ is the BS-RIS-AU link (or reflected link) which is modeled using a concatenation of three components: the BS-to-RIS channel, RIS reflection coefficient, and RIS-to-AU channel. The $\boldsymbol{h}_{b,\bar{u}_b}^H$ is the BS-to-AU link (or the direct link).

Due to fading effect and the RIS deployment structure, $\boldsymbol{g}_{r,\bar{u}_b}^H \boldsymbol{\Theta}_r^H \boldsymbol{F}_{b,r} = 0$, if $r \neq b$. This follows the fact that the RIS is deployed near to its associated BS and it is tilted upwards. Thus, it is very difficult to reflect signal from a neighboring BS $b$ to RIS $r$, where $r \neq b$. Furthermore, the considered RIS

[1]Note that additional RIS can be implemented to further enhance the user performance but this aspect is not considered here.

is tilted upward and thus it does not affect the TU. Therefore, the received signal of the TU $\underline{u}_b$ is

$$y_{\underline{u}_b} = \underbrace{\boldsymbol{h}_{b,\underline{u}_b}^H \boldsymbol{x}_b}_{\text{direct link}} + \underbrace{\sum_{c\neq b} \boldsymbol{h}_{b,\underline{u}_c}^H \boldsymbol{x}_c}_{\text{inter-cell interference}} + n_{\underline{u}_b}, \tag{2}$$

where $n_{\underline{u}_b} \sim \mathcal{CN}(0, N_0)$ is the additive white Gaussian noise (AWGN) at TU $\underline{u}_b$. In SDMA, each user treats the co-channel interference as noise. Therefore, the signal-to-interference-plus-noise (SINR) of TU $\underline{u}_b$ is

$$\text{SINR}_{\underline{u}_b}^{\text{SDMA}} = \frac{\left|\boldsymbol{h}_{b,\underline{u}_b}^H \boldsymbol{w}_{b,\underline{u}_b}\right|^2}{\underbrace{\sum_{v\neq \underline{u}_b} \left|\boldsymbol{h}_{b,\underline{u}_b}^H \boldsymbol{w}_{b,v}\right|^2}_{\text{intra-cell interference}} + \underbrace{\sum_{c\neq b}\sum_{\forall v} \left|\boldsymbol{h}_{c,\underline{u}_b}^H \boldsymbol{w}_{c,v}\right|^2}_{\text{inter-cell interference}} + N_0}, \tag{3}$$

and the SINR of AU $\bar{u}_b$ is

$$\text{SINR}_{\bar{u}_b}^{\text{SDMA}} = \frac{\left|\left(\boldsymbol{g}_{b,\bar{u}_b}^H \boldsymbol{\Theta}_b^H \boldsymbol{F}_{b,b} + \boldsymbol{h}_{b,\bar{u}_b}^H\right) \boldsymbol{w}_{b,\bar{u}_b}\right|^2}{I_{b,\bar{u}_b} + I_{c,\bar{u}_b} + N_0}. \tag{4}$$

where

$$I_{b,\bar{u}_b} = \underbrace{\sum_{v\neq \bar{u}_b} \left|\left(\boldsymbol{g}_{b,\bar{u}_b}^H \boldsymbol{\Theta}_b^H \boldsymbol{F}_{b,b} + \boldsymbol{h}_{b,\bar{u}_b}^H\right) \boldsymbol{w}_{b,v}\right|^2}_{\text{intra-cell interference}}, \tag{5}$$

$$I_{c,\bar{u}_b} = \underbrace{\sum_{c\neq b}\sum_{\forall v} \left|\left(\boldsymbol{g}_{c,\bar{u}_b}^H \boldsymbol{\Theta}_c^H \boldsymbol{F}_{c,c} + \boldsymbol{h}_{c,\bar{u}_b}^H\right) \boldsymbol{w}_{c,v}\right|^2}_{\text{inter-cell interference}}. \tag{6}$$

As seen later, it is also useful to rewrite (4) as follows:

$$\text{SINR}_{\bar{u}_b}^{\text{SDMA}} = \frac{\left|\boldsymbol{a}_b^H \boldsymbol{\Phi}_{b,\bar{u}_b,\bar{u}_b} + q_{b,\bar{u}_b,\bar{u}_b}\right|^2}{\tilde{I}_{b,\bar{u}_b} + \tilde{I}_{c,\bar{u}_b} + N_0}, \tag{7}$$

where $\boldsymbol{a}_b = \left[a_b^{(1)}, \ldots, a_b^{(N)}\right]^H$, $a_b^{(n)} = e^{j\theta_{b,n}}$, $n = 1, \ldots, N$, $\boldsymbol{\Phi}_{b,\bar{u}_b,v} = \text{diag}(\boldsymbol{g}_{b,\bar{u}_b}^H)\boldsymbol{F}_{b,b}\boldsymbol{w}_{b,v}$, and $q_{b,\bar{u}_b,v} = \boldsymbol{h}_{b,\bar{u}_b}^H \boldsymbol{w}_{b,v}$. In (7),

$$\tilde{I}_{b,\bar{u}_b} = \sum_{v\neq \bar{u}_b} \left|\boldsymbol{a}_b^H \boldsymbol{\Phi}_{b,\bar{u}_b,v} + q_{b,\bar{u}_b,v}\right|^2 = (5),$$

$$\tilde{I}_{c,\bar{u}_b} = \sum_{c\neq b}\sum_{\forall v} \left|\boldsymbol{a}_c^H \boldsymbol{\Phi}_{c,\bar{u}_b,v} + q_{c,\bar{u}_b,v}\right|^2 = (6).$$

The rate of a general user $u_b$ is

$$R_{u_b}^{\text{SDMA}} = \log\left(1 + \text{SINR}_{u_b}^{\text{SDMA}}\right). \tag{8}$$

### B. Problem Formulation

In this paper, we aim to maximize the WSR of the TUs by optimal coordinated beamforming and phase shift subject to the AUs' rate requirement.[2] The optimization problem is formulated as follows:

$$\max_{\boldsymbol{W},\boldsymbol{\Theta}} \quad \sum_{\forall \underline{u}_b, \forall b} \mu_{\underline{u}_b} R_{\underline{u}_b}^{\text{SDMA}}, \tag{9a}$$

$$\text{s.t.} \quad R_{\bar{u}_b}^{\text{SDMA}} \geq R_{\min}, \forall \bar{u}_b, \forall b, \tag{9b}$$

$$\sum_{\forall u_b \in \mathcal{U}_b} \|\boldsymbol{w}_{b,u_b}\|^2 \leq P_{\text{tx}}, \forall b, \tag{9c}$$

$$0 \leq \theta_{b,n} < 2\pi, \forall n, \forall b. \tag{9d}$$

where $\boldsymbol{W} = [\boldsymbol{W}_1, \ldots, \boldsymbol{W}_B]$, $\boldsymbol{W}_b = [\boldsymbol{w}_{b,1_b}, \ldots, \boldsymbol{w}_{b,U_b}]$, $\boldsymbol{\Theta} = [\boldsymbol{\Theta}_1, \ldots, \boldsymbol{\Theta}_B]$ are the optimization variables, $\mu_{\underline{u}_b}$ is the weight of TUs $\underline{u}_b$, and $P_{\text{tx}}$ is the maximum transmit power constraint at the BSs. The optimization problem (9) is very challenging to solve because the beamforming and phase shift variables are mutually coupled and thus the considered optimization problem is non-convex. Furthermore, due to the presence of intra-cell interference and ICI, the objective function (9a) and constraint (9b) are highly non-linear and non-convex.

## III. Optimal Coordinated Beamforming and Phase shift

In this section, we develop an efficient method to solve the non-convex optimization problem (9). Specifically, we employ alternating optimization (AO) as the primal method. The idea of AO is to optimize some decision variables while keeping the other decision variables fixed. This method allows us to decouple the non-convex problem into sub-problems. For the sub-problems, we then employ successive convex approximation (SCA) and semi-definite relaxation (SDR) to address non-convex challenges.

### A. Optimal Coordinated Beamforming

Suppose $\boldsymbol{\Theta}$ is fixed, then (9) is reduced to a coordinated beamforming problem. Specifically, it can be expressed as follows:

$$\max_{\boldsymbol{W}} \quad \sum_{\forall \underline{u}_b, \forall b} \mu_{\underline{u}_b} R_{\underline{u}_b}^{\text{SDMA}}, \tag{10a}$$

$$\text{s.t. } R_{\bar{u}_b}^{\text{SDMA}} \geq R_{\min}, \forall \bar{u}_b, \forall b, \tag{10b}$$

$$\sum_{\forall u_b} \|\boldsymbol{w}_{b,u_b}\|^2 \leq P_{\text{tx}}, \forall b. \tag{10c}$$

Due to the presence of interference, (10a) and (10b) are non-convex. To address the non-convexity, we introduce auxiliary variables and utilize the second-order cone representation. The optimization problem (10) can then be reformulated as:

[2]Unlike coordinated multi-point transmission, which requires the exchange of user messages, the proposed scheme only requires the exchange of channel state information.

$$\max_{\boldsymbol{W},\boldsymbol{\beta},\boldsymbol{\gamma}} \quad \sum_{\forall \underline{u}_b,\forall b} \mu_{\underline{u}_b} \log\left(1+\gamma_{\underline{u}_b}\right) \tag{11a}$$

$$\text{s.t.} \quad \sqrt{\gamma_{\underline{u}_b}\beta_{\underline{u}_b}} \le \left|\hat{\boldsymbol{h}}_{b,\underline{u}_b}^H \boldsymbol{w}_{b,\underline{u}_b}\right|, \forall \underline{u}_b, \forall b, \tag{11b}$$

$$\left\| \hat{\boldsymbol{h}}_{b,\underline{u}_b}^H \boldsymbol{W}_{b,-\underline{u}_b} \quad \boldsymbol{C}_{\underline{u}_b} \quad \sqrt{N_0} \right\| \le \sqrt{\beta_{\underline{u}_b}}, \forall \underline{u}_b, \forall b, \tag{11c}$$

$$\left\| \hat{\boldsymbol{h}}_{b,\bar{u}_b}^H \boldsymbol{W}_{b,-\bar{u}_b} \quad \boldsymbol{C}_{\bar{u}_b} \quad \sqrt{N_0} \right\| \le \sqrt{\frac{1}{\gamma_{\bar{u}_b}}} \left|\hat{\boldsymbol{h}}_{b,\bar{u}_b}^H \boldsymbol{w}_{b,\bar{u}_b}\right|, \forall \bar{u}_b, \forall b, \tag{11d}$$

$$\|\text{vec}\left(\boldsymbol{W}_b\right)\| \le \sqrt{P_{\text{tx}}}, \forall b. \tag{11e}$$

where $\hat{\boldsymbol{h}}_{b,\underline{u}_b}^H = \boldsymbol{h}_{b,\underline{u}_b}^H$, $\hat{\boldsymbol{h}}_{b,\bar{u}_b}^H = \left(\boldsymbol{g}_{b,\bar{u}_b}^H \boldsymbol{\Theta}_b^H \boldsymbol{F}_{b,b} + \boldsymbol{h}_{b,\bar{u}_b}^H\right)$, $\boldsymbol{\gamma} = [\gamma_{1_b}, \ldots, \gamma_{T_b}]$, $\gamma_{\bar{u}_b} = \left(2^{R_{\min}} - 1\right)$, and

$$\boldsymbol{W}_{b,-u_b} = \left[\boldsymbol{w}_{b,1_b}, \ldots, \boldsymbol{w}_{b,u_b-1}, \boldsymbol{w}_{b,u_b+1}, \ldots, \boldsymbol{w}_{b,U_b}\right],$$

$$\boldsymbol{C}_{u_b} = \left[\hat{\boldsymbol{h}}_{1,u_b}^H \boldsymbol{W}_1, \ldots, \hat{\boldsymbol{h}}_{b-1,u_b}^H \boldsymbol{W}_{b-1}, \hat{\boldsymbol{h}}_{b+1,u_b}^H \boldsymbol{W}_{b+1}, \ldots, \hat{\boldsymbol{h}}_{B,u_b}^H \boldsymbol{W}_B\right].$$

In (11), the auxiliary variable $\gamma_{\underline{u}_b}$ and $\beta_{\underline{u}_b}$ can respectively be interpreted as the SINR and the undesired signal (e.g. interference and noise) of user $\underline{u}_b$. Notice that by using such a representation, only the constraint (11b) remains to be non-convex. To relax this non-convex constraint, we further employ SCA. Specifically, the optimization problem (11) can be sequentially solved via the following problem:

$$\max_{\boldsymbol{W},\boldsymbol{\beta},\boldsymbol{\gamma}} \quad \sum_{\forall \underline{u}_b} \mu_{\underline{u}_b} \log\left(1+\gamma_{\underline{u}_b}\right), \forall b \tag{12a}$$

$$\text{s.t.} \quad \Re\left(\hat{\boldsymbol{h}}_{b,\underline{u}_b}^H \boldsymbol{w}_{b,\underline{u}_b}\right) \ge \sqrt{\gamma_{\underline{u}_b}^{(l)}\beta_{\underline{u}_b}^{(l)}} + \frac{1}{2}\sqrt{\frac{\beta_{\underline{u}_b}^{(l)}}{\gamma_{\underline{u}_b}^{(l)}}}\left(\gamma_{\underline{u}_b} - \gamma_{\underline{u}_b}^{(l)}\right) + \frac{1}{2}\sqrt{\frac{\gamma_{\underline{u}_b}^{(l)}}{\beta_{\underline{u}_b}^{(l)}}}\left(\beta_{\underline{u}_b} - \beta_{\underline{u}_b}^{(l)}\right), \forall \underline{u}_b, \forall b, \tag{12b}$$

$$(11c), (11d), (11e), \tag{12c}$$

where $\gamma_{u_b}^{(l)}$ and $\beta_{u_b}^{(l)}$ are the values of the optimal auxiliary variables obtained in the $(l-1)$th iteration. (12) is a convex optimization problem and thus it can be solved efficiently. Hence, the non-convex optimization problem (10) can be efficiently solved by sequentially solving the convex optimization problem (12).

### *B. Optimal Coordinated Phase shift*

Next, let us consider a coordinated phase shift problem. Suppose $\boldsymbol{W}$ is fixed, then (9) is reduced to the following problem:

$$\text{find} \quad \boldsymbol{\Theta}_b, \forall b, \tag{13a}$$

$$\text{s.t. } R_{\bar{u}_b}^{\text{SDMA}} \ge R_{\min}, \forall \bar{u}_b, \tag{13b}$$

$$0 \le \theta_{b,n} < 2\pi, \forall n, \forall b. \tag{13c}$$

Using the notation in (7), (13) can be rewritten as follows:

$$\text{find} \quad \boldsymbol{a}_b, \forall b, \tag{14a}$$

$$\text{s.t. } \left|\boldsymbol{a}_b^H \boldsymbol{\Phi}_{b,\bar{u}_b,\bar{u}_b} + q_{b,\bar{u}_b,\bar{u}_b}\right|^2 \ge \gamma_{\bar{u}_b}\left(\tilde{I}_{b,\bar{u}_b} + \tilde{I}_{c,\bar{u}_b} + N_0\right), \forall \bar{u}_b \in \bar{\mathcal{U}}_{\mathfrak{b}}, \forall b, \tag{14b}$$

$$\left|a_b^{(n)}\right| = 1, \forall n, \forall b. \tag{14c}$$

Owing to the presence of interference, (14b) is a non-convex constraint. Due to unit-modulus requirement, (14c) is also a non-convex constraint. To address the non-convexity, we use a similar argument as in [12]. Specifically, (14) is reformulated as follows:

$$\max_{\boldsymbol{A},\boldsymbol{\delta}} \quad \sum_{\forall b}\sum_{\forall \bar{u}_b} \delta_{b,\bar{u}_b}, \tag{15a}$$

$$\text{s.t. } \text{Tr}(\boldsymbol{\Psi}_{b,\bar{u}_b,\bar{u}_b}\boldsymbol{A}_b) + \left|q_{b,\bar{u}_b,\bar{u}_b}\right|^2 \ge \gamma_{\bar{u}_b}\sum_{v\neq\bar{u}_b}\text{Tr}(\boldsymbol{\Psi}_{b,\bar{u}_b,v}\boldsymbol{A}_b) + \gamma_{\bar{u}_b}\sum_{v\neq\bar{u}_b}\left|q_{b,\bar{u}_b,v}\right|^2 + \gamma_{\bar{u}_b}\sum_{c\neq b}\sum_{\forall v}\text{Tr}(\boldsymbol{\Psi}_{c,\bar{u}_b,v}\boldsymbol{A}_c) + \gamma_{\bar{u}_b}\sum_{c\neq b}\sum_{\forall v}\left|q_{c,\bar{u}_b,v}\right|^2 + \gamma_{\bar{u}_b}N_0 + \delta_{b,\bar{u}_b}, \forall \bar{u}_b, \forall b, \tag{15b}$$

$$\boldsymbol{A}_b \ge 0, \boldsymbol{A}_b^{(n,n)} = 1, \forall n, \forall b, \tag{15c}$$

$$\text{Rank}\left(\boldsymbol{A}_b\right) = 1, \forall b, \tag{15d}$$

where $\boldsymbol{\delta} = [\boldsymbol{\delta}_1, \ldots, \boldsymbol{\delta}_B]$, $\boldsymbol{\delta}_b = [\delta_{b,T_b+1}, \ldots, \delta_{b,U_b}]$, and the auxiliary variable $\delta_{b,\bar{u}_b}$ is interpreted as the SINR residual of the AU $\bar{u}_b$. In (15), $\boldsymbol{A}_b = \begin{bmatrix} \boldsymbol{a}_b \\ 1 \end{bmatrix}\begin{bmatrix} \boldsymbol{a}_b \\ 1 \end{bmatrix}^H$, $\boldsymbol{A}_b^{(n,n)}$ is the $n$-th row and column of $\boldsymbol{A}_b$, and

$$\boldsymbol{\Psi}_{b,\bar{u}_b,v} = \begin{bmatrix} \boldsymbol{\Phi}_{b,\bar{u}_b,v}\boldsymbol{\Phi}_{b,\bar{u}_b,v}^H & \boldsymbol{\Phi}_{b,\bar{u}_b,v}q_{b,\bar{u}_b,v}^H \\ q_{b,\bar{u}_b,v}\boldsymbol{\Phi}_{b,\bar{u}_b,v}^H & 0 \end{bmatrix}.$$

Because of the rank-one constraint, (15) is still a non-convex optimization problem. Nevertheless, we can employ SDR to address the non-convexity problem, i.e., to drop the non-convex constraint (15d). This reduces (15) into a semi-definite programming (SDP) problem, which is a convex optimization problem. However, SDR may not necessarily yield rank-one solutions. To address this issue, we extend the Gaussian random procedure (GRP) to obtain a feasible solution to (15). Specifically, we jointly generate $B$ rank-one solutions, i.e., $\xi_b^{(k)} \sim \mathcal{CN}\left(0, A_b\right), \forall b$, where $k = 1, \ldots, K$, and select a feasible-solution sample that maximizes the objective value of (15). This method provides a high-quality solution to the non-convex optimization problem (15), which is an equivalent problem of (13).

### *C. Alternating Optimization*

To solve the non-convex optimization problem in (9), we employ alternating optimization between the coordinated beamforming problem (12) and coordinated phase shift (15). Specifically, we denote the objective value of (9) as $f\left(\boldsymbol{W}^{(j-1)}, \boldsymbol{\Theta}^{(j-1)}\right)$ for an arbitrary feasible point $\left(\boldsymbol{W}^{(j-1)}, \boldsymbol{\Theta}^{(j-1)}\right)$, where $j \ge 1$. Furthermore, we denote the

**Algorithm 1** Alternating Optimization

1: Set outer iteration $j = 0$, and initialize a feasible $(\boldsymbol{W}^{(j)},\boldsymbol{\Theta}^{(j)})$
2: **Repeat**
3: Update $j := j + 1$
4: Given $\boldsymbol{\Theta}^{(j-1)}$, obtain $\boldsymbol{W}^{(j)}$using Algorithm 2
5: Given $\boldsymbol{W}^{(j)}$ , obtain $\boldsymbol{\Theta}^{(j)}$ using Algorithm 3
6: **Until** convergence or maximum iteration

**Algorithm 2** Successive Convex Approximation

1: Set inner iteration $l = 0$, and initialize $(\boldsymbol{\gamma}^{(l)},\boldsymbol{\beta}^{(l)})$
2: **Repeat**
3: Update $l := l + 1$
4: Obtain $\boldsymbol{W}^{(l)}, \boldsymbol{\gamma}, \boldsymbol{\beta}$ by solving (12)
5: Update $\boldsymbol{\gamma}^{(l)} := \boldsymbol{\gamma}_{u_b}$ and $\boldsymbol{\beta}^{(l)} := \boldsymbol{\beta}$
6: **Until** convergence or maximum iteration

objective value of (12) as $f_1\left(\boldsymbol{W}^{(j)},\boldsymbol{\Theta}^{(j-1)}\right)$, and its solution as $(\boldsymbol{W}^{(j)},\boldsymbol{\Theta}^{(j-1)})$ in the $j$-th iteration. As discussed above, (9) is equivalent to (12) for a fixed $\boldsymbol{\Theta}^{(j-1)}$. Therefore, we have: $f\left(\boldsymbol{W}^{(j)},\boldsymbol{\Theta}^{(j-1)}\right) = f_1\left(\boldsymbol{W}^{(j)},\boldsymbol{\Theta}^{(j-1)}\right) \geq f_1\left(\boldsymbol{W}^{(j-1)},\boldsymbol{\Theta}^{(j-1)}\right) = f\left(\boldsymbol{W}^{(j-1)},\boldsymbol{\Theta}^{(j-1)}\right)$. Furthermore, we denote the solution of (15) as $(\boldsymbol{W}^{(j)},\boldsymbol{\Theta}^{(j)})$ in the $j$-th iteration. As discussed above, (9) is equivalent to (15) for a fixed $\boldsymbol{W}^{(j)}$. Therefore, if $(\boldsymbol{W}^{(j)},\boldsymbol{\Theta}^{(j)})$ is a feasible solution in (15), it is also a feasible solution in (9). The objective value of (9) is not affected by a feasible $\boldsymbol{\Theta}^{(j)}$, thus we have $f\left(\boldsymbol{W}^{(j)},\boldsymbol{\Theta}^{(j)}\right) = f\left(\boldsymbol{W}^{(j)},\boldsymbol{\Theta}^{(j-1)}\right)$. Using these properties together, we then have: $f\left(\boldsymbol{W}^{(j+1)},\boldsymbol{\Theta}^{(j)}\right) \geq f\left(\boldsymbol{W}^{(j)},\boldsymbol{\Theta}^{(j)}\right) = f\left(\boldsymbol{W}^{(j)},\boldsymbol{\Theta}^{(j-1)}\right) \geq f\left(\boldsymbol{W}^{(j-1)},\boldsymbol{\Theta}^{(j-1)}\right)$. This property shows that the proposed AO algorithm is monotonically non-decreasing over the iterations. The proposed optimization algorithm is summarized in Algorithm 1-3.

## IV. Results and Discussions

In this section, we provide Monte-Carlo simulation results to analyze the performance gain of our proposed scheme. We consider three BSs at a fixed height of 25m and $M = 2$. Each RIS is located around the associated BS with a uniformly distributed angle, a fixed radius of 5m, and a fixed height of 20m. Each cell consists of an AU and a TU where the AU and TU are located at a fixed height of 120m and 1.5m, respectively. Unless stated otherwise, the 2D locations of the BSs, AUs, and TUs are shown in Fig. 2.

The pathloss of the BS-AU, BS-RIS, RIS-AU, and BS-TU links are modeled based on the distance-dependent path loss model [12]. The path loss at the reference point of 1m is $-30$dB, and the path loss exponent of the BS-AU, BS-RIS, RIS-AU, and BS-TU links are fixed at 2.1, 2.1, 2.1, and 4, respectively [6]. The mainlobe gain is 0dB and the sidelobe gain is $-20$dB [17]. Due to a high probability of LOS, the Rician K-factor of the Rician fading for BS-RIS, RIS-AU, and BS-AU links is 3dB. Due to a low probability of LOS, Rayleigh fading is considered for the BS-TU links.

For benchmarking purpose, we consider zero-forcing (ZF) precoding with optimal phase shift, optimal beamforming with random phase shift, and optimal beamforming without RIS as the baseline scheme. In the proposed algorithm, we initialize $\boldsymbol{W}^{(0)}$ and $\boldsymbol{\Theta}^{(0)}$ using maximal ratio transmission precoding and uniform distribution, respectively. $(\boldsymbol{\gamma}^{(0)},\boldsymbol{\beta}^{(0)})$ are initialized by replacing the inequalities in (11b) and (12b) with equality.

**Algorithm 3** SDP and GRP

1: Obtain $\boldsymbol{A}$ by solving the SDR of (15)
2: Generate $\xi_b^{(k)} \sim \mathcal{CN}\left(0, A_b\right), \forall b$, where $k = 1, \ldots, K$
3: Select a feasible $\text{sgn}(\boldsymbol{\xi}^{(k)})$ that maximizes the objective value of (15)

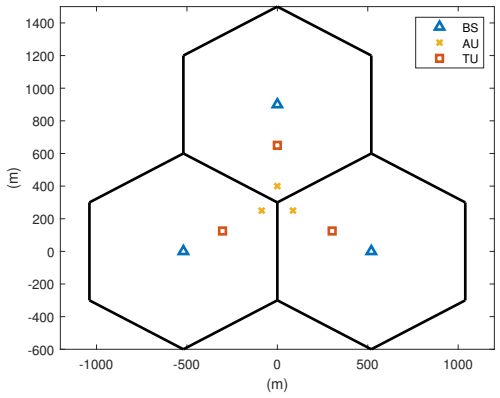


Figure 2. 2D locations of the BSs, AUs, and TUs.

Fig. 3 shows the WSR of the TUs versus the number of reflecting elements. As it is seen, our proposed scheme provides the highest WSR and it outperforms the baseline scheme without RIS by 48%. This indicates that the RIS can substantially minimize the ICI. Owing to power scaling law, the WSR of TUs in our proposed scheme also increases w.r.t. number of reflecting elements. Furthermore, ZF scheme achieves a higher WSR than that of random phase and baseline schemes. Nevertheless, due to fixed precoding, there are more instances where the solutions become infeasible.

Fig. 4 shows the WSR of the TUs versus horizontal distance of the AUs within the cell. Here, the AUs are located on the line segment between the associated BSs and the intersection of the three cells. Our results show that the proposed scheme obtains higher gains if the AUs are located nearer to their associated BSs. This is due to stronger desired signal and weaker ICI. In ZF scheme, the WSR of the TUs increases as the distance increases. This is because there are more realizations where the solutions are infeasible, resulting in the average being calculated from a smaller number of samples. Furthermore, as anticipated, optimal beamforming with random phase shifts and optimal beamforming without RIS exhibit similar performance, as the RIS is not well-utilized.

*Remark* 1. Implementing RIS in cellular-connected UAV is a challenging task. This is because the path loss of the reflected links suffers double fading effect. Interestingly, one can address this challenge by placing the RIS near to the BS.

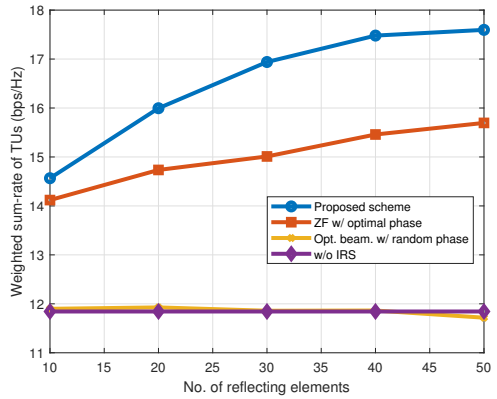


Figure 3. WSR of the TUs versus number of reflecting elements.

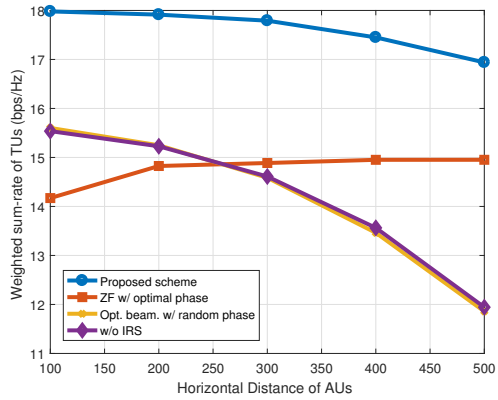


Figure 4. WSR of the TUs versus horizontal distance of the AUs, $N = 30$.

Furthermore, one can deploy the RIS within the mainlobe coverage of the BS and leverage the power scaling law to obtain stronger reflected links. If the reflected links are stronger than that of direct links, then RIS can reconfigure the channels and provide significant gains.

## V. Conclusion

In this paper, we investigated a coordinated RIS-aided cellular-connected UAV scheme designed to provide ubiquitous coverage in the sky and mitigate the strong ICI experienced by AUs, while prioritizing the performance of TUs. We developed an optimization algorithm to obtain the optimal coordinated beamforming and phase shift that maximized the WSR of the TUs subject to AUs' rate requirement. Our simulation results demonstrated that the coordinated RIS-aided cellular-connected UAV scheme is a promising solution, with the WSR of TUs increasing as the number of reflecting elements increased, all while satisfying the AUs' rate requirements. Compared to the baseline scheme without RIS, the proposed scheme delivered a WSR gain of up to 48%. Moreover, in this scheme, it is advantageous for AUs to be located closer to their associated BSs, as the RIS provides ubiquitous coverage in the sky and jointly mitigates strong ICI of the AUs.

## Acknowledgment

This work was supported by the Ministry of Higher Education Malaysia through the Higher Institution Centre of Excellence (HICOE) Grant 4J636, in part by Universiti Teknologi Malaysia under Grant 22H33 and in part by H2020-MSCA-RISE-2020 under Grant 101008085.

## References

[1] W. K. New and C. Y. Leow, "Unmanned aerial vehicle (UAV) in future communication system," in *2021 26th IEEE Asia-Pacific Conference on Communications (APCC)*, pp. 217–222, 2021.

[2] I. A. Meer, M. Ozger, D. A. Schupke, and C. Cavdar, "Mobility management for cellular-connected UAVs: Model-based versus learning-based approaches for service availability," *IEEE Transactions on Network and Service Management*, vol. 21, no. 2, pp. 2125–2139, 2024.

[3] W. K. New, C. Y. Leow, K. Navaie, and Z. Ding, "Robust non-orthogonal multiple access for aerial and ground users," *IEEE Transactions on Wireless Communications*, vol. 19, no. 7, pp. 4793–4805, 2020.

[4] H. Xu, C. Pan, K. Wang, M. Chen, and A. Nallanathan, "Resource allocation for UAV-assisted IoT networks with energy harvesting and computation offloading," in *2019 11th International Conference on Wireless Communications and Signal Processing (WCSP)*, pp. 1–7, 2019.

[5] W. K. New, C. Y. Leow, K. Navaie, Y. Sun, and Z. Ding, "Interference-aware NOMA for cellular-connected UAVs: Stochastic geometry analysis," *IEEE Journal on Selected Areas in Communications*, pp. 1–1, 2021.

[6] W. K. New, C. Y. Leow, K. Navaie, and Z. Ding, "Aerial-terrestrial network NOMA for cellular-connected UAVs," *IEEE Transactions on Vehicular Technology*, vol. 71, no. 6, pp. 6559–6573, 2022.

[7] W. Mei and R. Zhang, "Cooperative downlink interference transmission and cancellation for cellular-connected UAV: A divide-and-conquer approach," *IEEE Transactions on Communications*, vol. 68, no. 2, pp. 1297–1311, 2020.

[8] X. Mu, J. Xu, Y. Liu, and L. Hanzo, "Reconfigurable intelligent surface-aided near-field communications for 6G: Opportunities and challenges," *IEEE Vehicular Technology Magazine*, vol. 19, no. 1, pp. 65–74, 2024.

[9] F. R. Ghadi, M. Kaveh, and D. Martin, "Performance analysis of RIS/STAR-IOS-aided V2V NOMA/OMA communications over composite fading channels," *IEEE Transactions on Intelligent Vehicles*, vol. 9, no. 1, pp. 279–286, 2024.

[10] E. Shi, J. Zhang, H. Du, B. Ai, C. Yuen, D. Niyato, K. B. Letaief, and X. Shen, "RIS-aided cell-free massive MIMO systems for 6G: Fundamentals, system design, and applications," *Proceedings of the IEEE*, vol. 112, no. 4, pp. 331–364, 2024.

[11] S. Sharma, A. K. Mishra, M. H. Kumar, K. Deka, and V. Bhatia, "Intelligent reflecting surfaces (IRS)-enhanced cooperative NOMA: A contemporary review," *IEEE Access*, vol. 12, pp. 82168–82191, 2024.

[12] Q. Wu and R. Zhang, "Intelligent reflecting surface enhanced wireless network via joint active and passive beamforming," *IEEE Transactions on Wireless Communications*, vol. 18, no. 11, pp. 5394–5409, 2019.

[13] H. Xie, J. Xu, and Y.-F. Liu, "Max-min fairness in IRS-aided multi-cell MISO systems with joint transmit and reflective beamforming," *IEEE Transactions on Wireless Communications*, vol. 20, no. 2, pp. 1379–1393, 2021.

[14] L. Yang, F. Meng, J. Zhang, M. O. Hasna, and M. D. Renzo, "On the performance of RIS-assisted dual-hop UAV communication systems," *IEEE Transactions on Vehicular Technology*, vol. 69, no. 9, pp. 10385–10390, 2020.

[15] F. Rostami Ghadi, K.-K. Wong, W. K. New, H. Xu, R. Murch, and Y. Zhang, "On performance of RIS-aided fluid antenna systems," *IEEE Wireless Communications Letters*, vol. 13, no. 8, pp. 2175–2179, 2024.

[16] S. Jie Seah, C. Y. Leow, R. Nalinggam, W. Kiat New, R. Alam, S. Ling Jong, H. Yin Lam, and A. M. Almasoud, "Empirical channel models for UAV communication: A comparative study," *IEEE Access*, vol. 12, pp. 96740–96756, 2024.

[17] C. A. Balanis, *Antenna Theory: Analysis and Design, 3rd Edition*. John Wiley & Sons, 2005.